

Research article

Vegetation greening and driving factors in the Eurasian drylands under sustained drought conditions over recent two decades



Jinyue Liu^a, Chao Yue^{a,b,c}, Fan Yi^{a,b}, Pengyi Zhang^c, Junhao He^{a,b,*}, Jie Zhao^{d,**}

^a College of Soil and Water Conservation Science and Engineering, Northwest A & F University, Yangling, Shaanxi, 712100, China

^b State Key Laboratory of Soil and Water Conservation and Desertification Control, Northwest A & F University, Yangling, Shaanxi, 712100, China

^c College of Natural Resources and Environment, Northwest A & F University, Yangling, Shaanxi, 712100, China

^d Shandong Provincial Key Laboratory of Water and Soil Conservation and Environmental Protection, College of Resources and Environment, Linyi University, Linyi, Shandong, 276000, China

ARTICLE INFO

Keywords:

Vegetation dynamics
Environmental change
Anthropogenic activities
Satellite observation
Vegetation model
Eurasian drylands

ABSTRACT

Eurasian drylands constitute the largest contiguous arid and semi-arid region globally, where the ecosystems are particularly vulnerable to environmental changes and anthropogenic activities, posing threats to the sustainability of the regional vegetation. Therefore, quantifying vegetation dynamics and identifying their driving factors is crucial in environmental management and regulation. In this study, we evaluated the spatio-temporal dynamics of vegetation and their underlying drivers across Eurasian drylands during 2003–2020. The results show that the satellite-derived leaf area index (LAI) and gross primary production (GPP) exhibited consistently significant increasing trends. Conversely, soil moisture and terrestrial water storage declined over the same period, while significant increasing trends were found in temperature and vapor pressure deficit. Precipitation and surface net solar radiation showed non-significant increasing trends. Attribution analysis show that, irrespective of CO₂ fertilization effect, both environmental factors and anthropogenic activities contributed positively to vegetation greening, with anthropogenic activities playing the dominant role. Among the environmental drivers, water availability was identified as the most influential factor, accounting for over 50 % of the increase in vegetation greening. The reported overwhelming anthropogenic effect on regional vegetation greening, despite regional drying trend, raises concerns about the long-term sustainability of these ecosystems under future climate change. Therefore, close monitoring and early alerts regarding vegetation growth are imperative for the sustainable management of Eurasian dryland ecosystems.

1. Introduction

Drylands cover over 40 % of the terrestrial land surface and support approximately 38 % of the global population (Lian et al., 2021). Besides, they provide a wide range of essential ecosystem services, including food, energy, biodiversity, and carbon sequestration (Fu et al., 2021). The Eurasian drylands constitute the largest contiguous arid and semi-arid region in the world, playing a crucial role in maintaining the balance of the global ecosystem (Maestre et al., 2021; Zhang et al., 2023b). However, over the past decades, the ecosystems in this region have undergone substantial changes due to the combined influences,

both positive and negative of anthropogenic activities and environmental change (Huang et al., 2021; Liu et al., 2022). Nevertheless, most previous studies have focused on specific subregions within the Eurasian drylands, such as China (Liu et al., 2022), India (Banerjee et al., 2023), and Central Asia (Potapov et al., 2021). Few have examined the pathways and relative contributions of environmental change and anthropogenic activities to vegetation dynamics across the entire Eurasian drylands. Therefore, understanding and quantifying the long-term impacts of environmental change and anthropogenic activities on vegetation dynamics at the continental scale is crucial for policymakers to develop innovative conservation and land restoration strategies, thereby

* Corresponding author. College of Soil and Water Conservation Science and Engineering, Northwest A & F University, Yangling, Shaanxi, 712100, China.

** Corresponding author. Shandong Provincial Key Laboratory of Water and Soil Conservation and Environmental Protection, College of Resources and Environment, Linyi University, Linyi, Shandong, 276000, China.

E-mail addresses: junhaohe@nwafu.edu.cn (J. He), sxuzhaojie@163.com (J. Zhao).

supporting regional ecosystem services and human livelihood.

In recent years, a variety of vegetation indices have been developed to investigate vegetation dynamics in dryland ecosystems (Chen et al., 2024a; Wang et al., 2023). Among them, the Leaf Area Index (LAI) indicates the total leaf surface area available for photosynthesis, while gross primary production (GPP) quantifies the amount of carbon assimilated by plants through photosynthesis over a given time period. These two indices reflect the intermediate process and ultimate product of vegetation photosynthesis, respectively (Liu et al., 2023; Yao et al., 2020). Among numerous remote sensing data products, LAI and GPP derived from the Moderate Resolution Imaging Spectroradiometer (MODIS) are widely used due to their advantages such as easy acquisition, long time series, and stable data quality (Liu et al., 2023). Therefore, they have been extensively used in vegetation dynamic monitoring at the national and regional scales, such as China (Liu et al., 2022), Central Asia (Guo et al., 2024), China's Loess Plateau (Tian et al., 2024). Although satellite monitoring products provide convenience for vegetation dynamics analysis, quantifying and identifying the drivers behind such dynamics remains challenging, especially due to the complex interactions between environmental and anthropogenic factors.

Vegetation in drylands performs multiple ecosystem functions, such as preventing soil erosion, maintaining soil moisture, and increasing carbon storage (Ding et al., 2020; Zhang et al., 2023a). However, the global climate change may influence these functions through a complex interplay of environmental factors, including temperature, precipitation, soil moisture (SM), terrestrial water storage (TWS), vapor pressure deficit (VPD), and surface net solar radiation (SSRD), by regulating vegetation phenology, distribution, productivity, and other characteristics of vegetation (Li et al., 2015; Liu et al., 2023). Among these factors, precipitation, temperature, and SSRD have been widely recognized as key climate drivers controlling vegetation dynamics in Eurasian drylands. Since the 1980s, the warming rate in the Eurasian drylands has been evidently higher than the global average (Zhang et al., 2023b). This increase in temperature promoted the potential evapotranspiration. Combined with fluctuating precipitation, this has resulted in a continuous decline in regional water (Maestre et al., 2021; Zhang et al., 2020). Zhang et al. (2020) reported that the changes in hydrothermal conditions (i.e., temperature and precipitation) affected aboveground net primary production of various vegetation types in Eurasian grasslands. Additionally, there are increasing concerns about the impacts of SM, VPD, and TWS on vegetation dynamics (Deng and Chen, 2017; Zhang et al., 2023b). For example, Wang et al. (2022) found that, when excluding the effects of main climatic drivers (e.g. air temperature, incoming shortwave radiation, and wind speed), VPD was more important for plant water stress than SM across most plant functional types. In contrast, Liu et al. (2023) argued that changes in vegetation dynamics in arid grasslands and shrublands were more sensitive to SM than to precipitation and VPD. Furthermore, CO₂ fertilization effect, which enhances plant photosynthesis, has been proven to be one of the major drivers of the vegetation greening in drylands (Chen et al., 2024b). The long-term physiological response is governed by limitations in ribulose 1,5-bisphosphate (RuBP) regeneration (Franks et al., 2013). However, this driver is often overlooked in studies of arid regions, leading to a conflation of the CO₂ fertilization effect with other environmental factors in attribution analysis (Liu et al., 2022; Yu et al., 2025; Zhang et al., 2024a).

The impacts of anthropogenic activities on Eurasian drylands ecosystems have notably emerged since the Second Industrial Revolution, with the negative effects such as excessive use of water resources, overgrazing, and deforestation. Concurrently, there have been positive activities, including ecosystem restoration and land management (Huang et al., 2021; Liu et al., 2022). Various studies have assessed the contribution of anthropogenic activities to vegetation dynamics across various spatial and temporal scales (Li et al., 2021; Park et al., 2023). At the national scale, anthropogenic activities accounted for more than 70 % to the increase in the normalized difference vegetation index (NDVI)

and gross primary productivity (GPP) in China from 1988 to 2018 (Liu et al., 2022). In Kazakhstan, crop production (59 %) and population density (48 %) significantly influenced vegetation dynamics from 2000 to 2016 (Venkatesh et al., 2022). At the regional scale, anthropogenic activities played a dominant role over any sole climate factors (temperature, precipitation, and radiation), accounting for 15.5 % of grasslands in the Tibetan Plateau from 2000 to 2016 (Wu et al., 2021). In northwest India, 79 % of the reduction in the Enhanced Vegetation Index (EVI) in lowland areas was attributed to negative impacts of anthropogenic activities such as deforestation from 2000 to 2016 (Banerjee et al., 2023). However, some anthropogenic interventions, such as inappropriate revegetation, overgrazing, and urban expansion have been shown to reduce vegetation productivity (Feng et al., 2016; Hao et al., 2021). While most existing studies focus on specific regions within Eurasian drylands, few have examined anthropogenic effects across the entire Eurasian drylands. In the long term, a better understanding of the human impact on dryland ecosystems can provide recommendations for land management and international government cooperation among Eurasian countries to achieve global sustainable development goals.

A variety of statistical methods have been developed and tested with the aim of separating the complex interactions between environmental drivers and anthropogenic activities (e.g., principal component analyses (Yao et al., 2018), correlation metrics (Liu et al., 2015), and residuals-trend modeling (RESTREND) (Bai et al., 2025). Among them, the RESTREND has emerged as a reliable and widely applied approach for separating the actual contributions of environmental factors and anthropogenic activities to vegetation dynamics across spatial scales (Xie et al., 2020). For example, Shi et al. (2021) used residual analysis to explore the causes of vegetation dynamics in China's Loess Plateau, while Pei et al. (2021) employed this method to distinguish the relative contributions of climate change and anthropogenic activities to NDVI changes. Therefore, in the long-term spatiotemporal analysis of vegetation dynamics, separating the CO₂ fertilization effect and applying RESTREND analysis enables more accurate attribution of vegetation trends to environmental and anthropogenic drivers.

Projected future climate change scenarios indicate that the Eurasian drylands will experience notable increases in temperature and aridity in the future (Zhang et al., 2024b). Therefore, it is imperative to examine Eurasian drylands vegetation dynamics and identify their drivers. Here, we evaluated the spatiotemporal patterns of vegetation dynamics in Eurasian drylands from 2003 to 2020 using satellite-observed LAI and GPP datasets, both before and after removing the CO₂ fertilization effect. Then, we assessed the relationships between vegetation dynamics (excluding CO₂ fertilization effect) and environmental variables (i.e. annual mean temperature (MAT), annual mean precipitation (MAP), SM, TWS, VPD, and SSRD) using partial correlation analysis. Finally, the contributions of environmental changes and anthropogenic activities to vegetation dynamics (after removing the CO₂ fertilization effect) were quantified using RESTREND analysis. The objectives of this study were to: 1) analyze the spatiotemporal LAI and GPP dynamics of Eurasian drylands during 2003–2020; 2) examine the impacts of the ongoing CO₂ fertilization effect and environmental factors on vegetation dynamics, and 3) quantitatively determine the contributions of environmental factors and anthropogenic activities to LAI and GPP tendencies in the Eurasian drylands.

2. Material and methods

2.1. Study area

The Eurasian drylands ($-20^{\circ}\text{W} \sim 180^{\circ}\text{E}$, $-10^{\circ}\text{S} \sim 80^{\circ}\text{N}$) constitute the world's largest arid region (Fig. 1), covering approximately $5.1 \times 10^7 \text{ km}^2$ (Maestre et al., 2021). In this study, the spatial extent of Eurasian drylands was delineated using the aridity index (AI), calculated as the ratio of annual precipitation to annual potential evapotranspiration. The

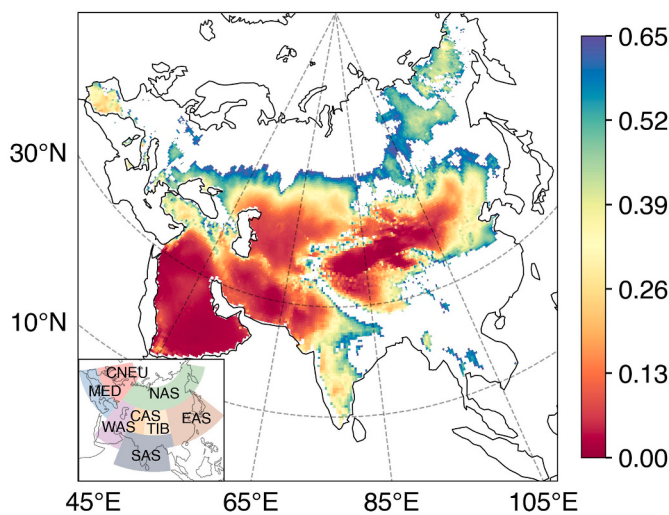


Fig. 1. The aridity index in Eurasian drylands. The inset charts show are South Asia (SAS), East Asia (EAS), Tibetan Plateau (TIB), Central Asia (CAS), West Asia (WAS), North Asia (NAS), Mediterranean (MED), and Central and North Europe (CNEU).

AI quantifies the balance between the atmospheric water supply and the potential demand of the land surface, providing an important insight into the water availability across the region (Zhang et al., 2024b). The AI for Eurasian region was derived from the global aridity database provided by the Consultative Group for International Agriculture Research Consortium for Spatial Information (CGIAR-CSI) with the spatial resolution of 30 arc seconds (Jiao et al., 2021), and then the data were aggregated to $0.5^\circ \times 0.5^\circ$ using bilinear interpolation algorithm to match the spatial resolution of environmental variables and vegetation indices products (see section 2.3). Accordingly, the Eurasian drylands were regions having AI below 0.65 (Maestre et al., 2021). Furthermore, to explore the effects of environmental variables and anthropogenic activities on the spatial and temporal changes on vegetation across different areas of the Eurasian drylands, we divided the Eurasian region into eight subregions according to the Intergovernmental Panel on Climate Change (IPCC) Special Report on Managing the Risks of Extreme Events and Disasters to Advance Climate Change Adaptation (SREX) reports (Field et al., 2012), namely South Asia (SAS), East Asia (EAS), Tibetan Plateau (TIB), Central Asia (CAS), West Asia (WAS), North Asia (NAS), Mediterranean (MED), and Central and North Europe (CNEU) (Fig. 1). The land cover data, with a spatial resolution of 300 m, were obtained from the European Space Agency's Climate Change Initiative (ESA CCI). To enhance the robustness of the results, this study focuses exclusively on vegetation cover types that remained unchanged from 2003 to 2020 (Fig. S1). The vegetation categories were reclassified into three types: woody, grassland, and cropland (Table S3).

2.2. Data collation

2.2.1. Environmental changes in the Eurasian drylands

The environmental changes in the Eurasian drylands were characterized by six variables, i.e., mean annual temperature (MAT), mean annual precipitation (MAP), surface solar radiation downwards (SSRD), soil moisture (SM), terrestrial water storage (TWS), and vapor pressure deficit (VPD). Monthly MAT and MAP at a spatial resolution of 0.5° from 2003 to 2020 were derived from the Climate Research Unit (CRU) TS v4.05 datasets of the Center for Environmental Data Analysis (CEDA) (Harris et al., 2020). Monthly SSRD was obtained from the European Reanalysis Interim v5 (ERA5) dataset at a spatial resolution of 0.1° for 2003–2020. The original unit of SSRD in joules per square meter ($J\text{ m}^{-2}$) was converted to watts per square meter (W m^{-2}) by dividing the accumulated values by the accumulation period in seconds

(Muñoz-Sabater et al., 2021). SM datasets were obtained as the depth-weighted mean values of the four soil layers within a 2-m depth from the Global Land Data Assimilation System (GLDAS) Noah SM products (Rodell et al., 2004), which have a spatial resolution of 0.25° and cover the period from 2003 to 2020 on a 3-h basis (Wu et al., 2023). Monthly TWS data were obtained from the Gravity Recovery and Climate Experiment (GRACE) level RL06 dataset (available from 2003 to 2017) (Watkins et al., 2015), and the GRACE Follow-On (GRACE-FO) dataset (2018–2020) (Landerer et al., 2020). Those two datasets provide gridded global TWS anomalies relative to the monthly average from 2004 to 2009 at a spatial resolution of 3° and scaled uncertainty estimates. Missing values in the GRACE series, including an approximately one-year gap between GRACE and GRACE-FO, were supplemented using linear interpolation (Hu et al., 2025). VPD was calculated using Eq. (1) on pixel-level at the 0.5° resolution using actual vapor pressure, maximum and minimum air temperatures obtained from the CRU TS v4.05 dataset for 2003–2020.

$$\begin{aligned} \text{VPD} = 0.5 \times & \left(0.611 \times \exp \left(\frac{17.3 \times \text{TEM}_{\min}}{\text{TEM}_{\min} + 237.3} \right) \right. \\ & \left. + 0.611 \times \exp \left(\frac{17.3 \times \text{TEM}_{\max}}{\text{TEM}_{\max} + 237.3} \right) \right) - \text{AVP}, \end{aligned} \quad (1)$$

where TEM_{\max} and TEM_{\min} are the maximum and minimum air temperatures ($^\circ\text{C}$), respectively, and AVP is the actual vapor pressure (kPa).

In this study, the subsequent analysis was conducted using annual values of six environmental variables mentioned above. Annual MAT, VPD, SM, and TWS were calculated by averaging their corresponding monthly values for all years from 2003 to 2020. Annual MAP and SSRD were calculated by summing the monthly values for each year. All environmental datasets retained values within the valid range as suggested by Harris et al. (2020), Rodell et al. (2004), Muñoz-Sabater et al. (2021), and Landerer et al. (2020), and resampled to 0.5° resolution using the bilinear interpolation algorithm. Finally, the regional and pixel-level averaged values for each environmental variable were derived from the fitted slopes using linear regression analysis to evaluate environmental changes across the Eurasian drylands.

2.2.2. Vegetation indices datasets

The leaf area index (LAI) and gross primary production (GPP) were used in this study to quantify vegetation dynamics in the Eurasian drylands (Table S1). In particular, the satellite-observed LAI and GPP were obtained from MOD15A2H and MOD17A2H of the Moderate Resolution Imaging Spectroradiometer (MODIS) product with a 500-m spatial resolution and 8-day temporal intervals, covering the period from 2003 to 2020 (Liu et al., 2023). The observations of LAI were first processed by combining the valid values (i.e. $\text{LAI} > 0$) with a scaling factor 0.1 from Myneni et al. (2021), and then the monthly LAI values were extracted through the maximum value composite (MVC) method. Eventually, the annual LAI was calculated as the average of monthly values within a year. The observed GPP were post-processed by combining the valid values (i.e. $\text{GPP} > 0$) with a scaling factor 0.0001 from Running et al. (2021), and then the monthly GPP was derived by the maximum value composite (MVC) method. Annual GPP values were calculated as the sums of monthly values within a year. In addition, to evaluate the influences of CO_2 fertilization effects on vegetation dynamics (see section 2.3.1), model-simulated LAI and GPP from S0 (no forcing), S1 (CO_2 only), and S3 (CO_2 , climate, and land use change) scenarios were obtained from 16 Dynamic Global Vegetation Models (DGVMs) (listed in Table S2) from the 'Trends in the Land Carbon Cycle' (TRENDY-v10) project for 2003–2020 (Yang et al., 2022). All datasets of vegetation dynamic variables were resampled to a 0.5° resolution using a bilinear interpolation algorithm. Similar to the environmental variables, regionally averaged and per-pixel vegetation variables were derived using linear regressions with time.

2.3. Methods

2.3.1. Contributions of CO₂ fertilization effect on vegetation dynamics

We adopted the concept of relative CO₂ assimilation rate ($A_{n(\text{rel})}$) with TRENDY simulated GPP and LAI to quantify the impact of CO₂ fertilization effect on the changes in MODIS GPP and LAI products (i.e., vegetation dynamics) between 2003 and 2020 (Burrell et al., 2020; Franks et al., 2013). In general, $A_{n(\text{rel})}$ describes the ratio of measured assimilation rate (A_n) at the measured CO₂ level (C_0) to that (A_0) measured at ambient (or reference) CO₂ concentration (C_{a0}), which links the increase in photosynthesis to increasing CO₂ (Reichgelt and D'Andrea, 2019). We assumed that the relative changes in MODIS GPP and LAI products due CO₂ fertilization effect from 2003 to 2020 are equal to those in TRENDY products, respectively, thus, $A_{n(\text{rel})}^{\text{MODIS}} = A_{n(\text{rel})}^{\text{TRENDY}}$. Thereby, the rescaled MODIS GPP and LAI excluding CO₂ fertilization effect for each year after 2003 can be obtained by,

$$\text{MODIS}_{\text{adj}}^i = \frac{\text{MODIS}_{\text{obs}}^i}{A_{n(\text{rel})}}, \quad (2)$$

where MODIS_{obs}ⁱ refers to the observed values of GPP/LAI in the i th year, whereas MODIS_{adj}ⁱ refers to the GPP/LAI values in the i th year after removing the CO₂ fertilization effect. $A_{n(\text{rel})}$ is calculated using TRENDY simulation results, as giving by,

$$A_{n(\text{rel})} = \frac{S3^i}{S3^{2003}}, \quad (3)$$

where $S3^i$ represents i th year GPP/LAI results from S3 simulation based on i th year climate forcing (Climate^i), atmospheric CO₂ (CO_2^i), and land use change (LUC^i), that is,

$$S3^i = \text{CO}_2^i + \text{Climate}^i + LUC^i, \quad (4)$$

In Eq. (3), $S3^{2003}$ represents simulation results at 2003 based on CO_2^{2003} , Climate^i , and LUC^i , expressed as,

$$S3^{2003} = \text{CO}_2^{2003} + \text{Climate}^i + LUC^i, \quad (5)$$

The difference between $S3^i$ and $S3^{2003}$ is $\Delta\text{CO}_2^{i-2003}$, which represents the CO₂ fertilization effects between i th year and 2003. The TRENDY protocol, however, does not have such simulation as described in Eq. (5). Alternatively, the difference between $S3^{2003}$ and $S3^i$ gives,

$$\begin{aligned} S3^{2003} - S3^i &= \text{CO}_2^{2003} + \text{Climate}^i + LUC^i - (\text{CO}_2^{2003} + \text{Climate}^{2003} + LUC^{2003}) \\ &= \Delta\text{Climate}^{i-2003} + \Delta LUC^{i-2003}, \end{aligned} \quad (6)$$

To find $\Delta\text{Climate}^{i-2003} + \Delta LUC^{i-2003}$, we first get the difference between $S3^i$ and $S1^{2003}$,

$$\Delta S3^{i-2003} = S3^i - S1^{2003} = \Delta\text{CO}_2^{i-2003} + \Delta\text{Climate}^{i-2003} + \Delta LUC^{i-2003}, \quad (7)$$

which yields,

$$\Delta\text{Climate}^{i-2003} + \Delta LUC^{i-2003} = S3^i - S1^{2003} - \Delta\text{CO}_2^{i-2003}, \quad (8)$$

$\Delta\text{CO}_2^{i-2003}$ can be find by calculating the difference between $S1^i$ and $S1^{2003}$,

$$\Delta S1^{i-2003} = S1^i - S1^{2003} = \Delta\text{CO}_2^{i-2003}, \quad (9)$$

In S1 simulation, there is i year difference of preindustrial climate effect between $S1^i$ and $S1^{2003}$, which can be eliminated using S0 simulation ($S0^i - S0^{2003}$). Then Eq. (9) is corrected as,

$$\Delta S1^{i-2003} = S1^i - S1^{2003} = \Delta\text{CO}_2^{i-2003} + (S0^i - S0^{2003}), \quad (10)$$

which yields,

$$\Delta\text{CO}_2^{i-2003} = S1^i - S1^{2003} - S0^i + S0^{2003}, \quad (11)$$

Substitute Eq. (11) into Eq. (8) gives,

$$\begin{aligned} \Delta\text{Climate}^{i-2003} + \Delta LUC^{i-2003} &= S3^i - S3^{2003} - \Delta\text{CO}_2^{i-2003} \\ &= S3^i - S3^{2003} - (S1^i - S1^{2003} - S0^i + S0^{2003}) \end{aligned} \quad (12)$$

Substitute Eq. (12) into Eq. (6) gives,

$$\begin{aligned} S3^{2003} - S3^i &= \Delta\text{Climate}^{i-2003} + \Delta LUC^{i-2003} = S3^i - S3^{2003} \\ &\quad - (S1^i - S1^{2003} - S0^i + S0^{2003}), \end{aligned} \quad (13)$$

Hence,

$$\begin{aligned} S3^{2003} &= S3^{2003} + \Delta\text{Climate}^{i-2003} + \Delta LUC^{i-2003} = S3^{2003} \\ &\quad + S3^i - S3^{2003} - (S1^i - S1^{2003} - S0^i + S0^{2003}) = S3^i \\ &\quad - ((S1^i - S1^{2003}) - (S0^i - S0^{2003})), \end{aligned} \quad (14)$$

Eventually, Eq. (3) can be corrected as,

$$A_{n(\text{rel})} = \frac{S3^i}{S3^{2003}} = \frac{S3^i}{S3^i - ((S1^i - S1^{2003}) - (S0^i - S0^{2003}))}, \quad (15)$$

Finally, the rescaled MODIS estimates (MODIS_{adj}: LAI_{adj} or GPP_{adj}) that exclude the CO₂ fertilization effect can be obtained by the following equation (Fig. S2 and Fig. S3),

$$\text{MODIS}_{\text{adj}}^i = \text{MODIS}_{\text{obs}}^i * \frac{S3^i - ((S1^i - S1^{2003}) - (S0^i - S0^{2003}))}{S3^i}, \quad (16)$$

2.3.2. Trend analysis

We calculated the Pearson correlation coefficients to assess the relationships between environmental variables (MAT, MAP, SM, TWS, VPD, and SSRD) and vegetation indices (GPP/LAI) over time to obtain regional averages and per-pixel variations in the Eurasian drylands from 2003 to 2020. A p -value <0.05 was considered significant.

2.3.3. Partial correlation analysis

Partial correlation analysis was used to determine the individual impacts of environmental factors on vegetation dynamics, excluding the confounding effects of other related variables. The significance of these partial coefficients was evaluated when the $p < 0.05$. The dominant factor was identified as the variable with the highest partial correlation coefficient after controlling for the influence of the remaining variables.

2.3.4. Contributions of environmental factors and anthropogenic activities to the temporal variability of vegetation

The contributions of environmental driving factors and anthropogenic activities to the trends in LAI_{adj} and GPP_{adj} at regional, subregional, and pixel scales were quantified using residual trend analysis (RESTREND) (Liu et al., 2022). Initially, the multiple linear regression was conducted between vegetation dynamics and environmental

variables (Eq. (17)).

$$Y = \hat{\beta}X + c, \quad (17)$$

where Y is a $n \times 1$ matrix representing the observed variable, where n is the number of observations; X represents a $n \times p$ matrix, where p is the number of predictor variables, $\hat{\beta}$ is a $p \times 1$ vector of the unknown coefficients, c is an $n \times 1$ vector the random errors.

The least squares estimate of $\hat{\beta}$ is as follows:

$$\hat{\beta} = (X'X)^{-1}X'Y, \quad (18)$$

However, during multiple linear regression analysis, the correlations between the independent variables (i.e., the environmental factors), also known as multicollinearity ($XX \approx 0$), must be properly addressed to enhance the explainability of the regression model (Bai et al., 2025). Accordingly, we employed the ridge regression, which adds a small perturbation, λI , to the least squares estimate, to eliminate multicollinearity among variables (Eq. (19)), thereby addressing the issue of non-invertibility of the generalized inverse.

$$\hat{\beta}(k) = (X'X + \lambda I)^{-1} X'Y, \quad (19)$$

The RESTREND procedure is outlined as follows, Firstly, each of the vegetation (LAI_{adj} or GPP_{adj}) and environmental variables (MAT, MAP, SM, TWS, VPD, and SRRD) was z-normalized to standardize the scales and mitigate the influences of disparate measurement units.

$$Z_{(ij)} = \frac{x_{(ij)} - \bar{x}_{(ij)}}{\sigma_{(ij)}}, \quad (20)$$

where $Z_{(ij)}$ is the variable j standard for a year i , $x_{(ij)}$ is the value of variable j for a year i , $\bar{x}_{(ij)}$ and $\sigma_{(ij)}$ is the average and standard deviation of variable j from 2003 to 2020, respectively.

Secondly, ridge regression was performed to quantify the sensitivities of LAI_{adj} and GPP_{adj} to each of the environmental variables:

$$VI_{nl} = \sum_{i=1}^n a_i X_{nl} + b, \quad (21)$$

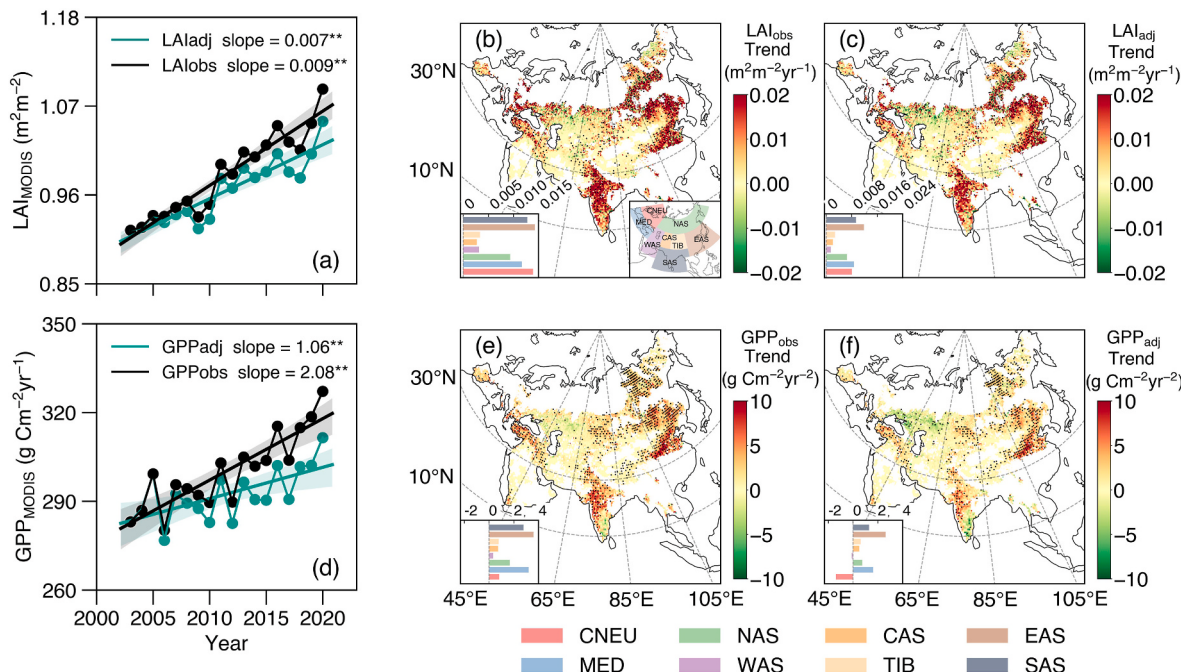


Fig. 2. The temporal trends of LAI (a, b, c), GPP (d, e, f) in Eurasian drylands at regional and pixel scale from 2003 to 2020. The colors of bars in inset charts indicate different regions as is shown in lower right of Fig. 2b. Note: the “*” and “**” indicates $p < 0.05$ and $p < 0.01$. The statistically significant regions ($p < 0.05$) are labeled with black spots.

where VI_{nl} is the normalized LAI_{adj} or GPP_{adj} obtained by Eq. (20), X_{nl} are the normalized environmental variables obtained by Eq. (20), a_i and b are the standard ridge regression coefficients, with i stands for each year from 2003 to 2020.

Subsequently, the actual contributions of environmental factors to LAI_{adj} and GPP_{adj} (Q_{ac}) were quantified using regression parameters a_i and the trend of environmental factors:

$$Q_c = \sum_{i=1}^n a_i X_{nl_trend,i}, \quad (22)$$

$$Q_{ac} = \frac{Q_c}{VI_{nl_trend}} \times VI_{trend}, \quad (23)$$

where Q_c refers to the contribution of environmental changes to the trends of the normalized vegetation variables, $X_{nl_trend,i}$ is the trend of a normalized single environmental variable, VI_{nl_trend} is the trend of normalized vegetation variables, and VI_{trend} is the actual temporal trend of the vegetation variables.

Finally, the actual contribution of anthropogenic activities (Q_{ah}) to the trend of LAI_{adj} and GPP_{adj} was determined by subtracting the contribution of environmental variables from the overall trends in the LAI_{adj} and GPP_{adj} :

$$Q_{ah} = VI_{trend} - Q_{ac}, \quad (24)$$

Note that, using residual analysis (Eq. (24)), this study quantifies all direct anthropogenic-induced ecosystem changes as anthropogenic effects. In other words, the anthropogenic effects include both positive (e.g., reforestation, forest, and crop management) and negative effects (e.g., land-use change) of anthropogenic activities.

3. Results

3.1. Vegetation dynamics in the Eurasian drylands during 2003–2020

The vegetation dynamics, indicated by LAI and GPP, in the Eurasian drylands during 2003–2020 were explored. Throughout the entire

Eurasian region, the original satellite-observed LAI_{obs} and GPP_{obs} showed a significant increasing trend ($p < 0.05$) over the study period, with the average rate of increase being $0.009 \text{ m}^2 \text{ m}^{-2} \text{ yr}^{-1}$ and $2.08 \text{ g C m}^{-2} \text{ yr}^{-2}$, respectively (Fig. 2a and d). At the pixel scale, 30.2 % and 37.3 % of the Eurasian drylands exhibited significant increases ($p < 0.05$) in LAI_{obs} and GPP_{obs} , respectively (Fig. 2b and e). Similar trends were observed for the entire Eurasian region when CO_2 fertilization effects were excluded from LAI_{obs} and GPP_{obs} , with the adjusted values, LAI_{adj} and GPP_{adj} , showing significant increases by $0.007 \text{ m}^2 \text{ m}^{-2} \text{ yr}^{-1}$ and $1.06 \text{ g C m}^{-2} \text{ yr}^{-2}$, respectively. At the subregional scale, the trends in LAI and GPP exhibited spatial variations across the Eurasian region. Among the 8 subregions, the trends of LAI_{obs} and LAI_{adj} showed significant increases, with the highest rates observed in EAS (0.014 and $0.012 \text{ m}^2 \text{ m}^{-2} \text{ yr}^{-1}$), SAS (0.013 and $0.010 \text{ m}^2 \text{ m}^{-2} \text{ yr}^{-1}$), CNEU (0.014 and $0.008 \text{ m}^2 \text{ m}^{-2} \text{ yr}^{-1}$), and MED (0.012 and $0.009 \text{ m}^2 \text{ m}^{-2} \text{ yr}^{-1}$). LAI_{obs} and LAI_{adj} had negative trend in Central Asia. Furthermore, GPP_{obs} and GPP_{adj} also exhibited high significant increasing rates, particularly in EAS (3.59 and $2.64 \text{ g C m}^{-2} \text{ yr}^{-2}$), MED (3.20 and $1.62 \text{ g C m}^{-2} \text{ yr}^{-2}$), and SAS (2.79 and $1.30 \text{ g C m}^{-2} \text{ yr}^{-2}$). However, CNEU and WAS showed negative trend of GPP_{adj} (GPP_{adj} : $-1.38 \text{ g C m}^{-2} \text{ yr}^{-2}$ of the CNEU, $-0.11 \text{ g C m}^{-2} \text{ yr}^{-2}$ of the WAS) (Fig. 2c and f).

3.2. Environmental changes in the Eurasian drylands during 2003–2020

The environmental changes within the Eurasian drylands from 2003 to 2020 were explained by six environmental factors (i.e., MAT, MAP, SM, TWS, VPD, and SSRD) at both the regional, subregional, and pixel scales. At the regional scale, MAT and VPD showed significant increases during 2003–2020, at rates of $0.03 \text{ }^\circ\text{C yr}^{-1}$ ($p < 0.05$) and $0.003 \text{ kPa yr}^{-1}$ ($p < 0.05$), respectively (Fig. 3a and e). MAP and SSRD also exhibited increasing trends at rates of 0.96 mm yr^{-2} and $0.33 \text{ W m}^{-2} \text{ yr}^{-1}$, respectively, but these increases were not statistically significant ($p > 0.05$) (Fig. 3b and f). Conversely, SM and TWS showed significant decrease trends during 2003–2020 at rates of $-0.001 \text{ m}^3 \text{ m}^{-3} \text{ yr}^{-1}$ ($p < 0.05$) and -3.70 mm yr^{-1} ($p < 0.05$), respectively (Fig. 3c and d). At the pixel and subregional scale, 94.43 % of the Eurasian drylands experienced increases in MAT, with more than 40.0 % of the area showed significant increases ($p < 0.05$) during 2003–2020. CNEU and NAS were the two subregions showing the largest and the second largest increase, with the increasing rate being $0.08 \text{ }^\circ\text{C yr}^{-1}$ and $0.09 \text{ }^\circ\text{C yr}^{-1}$,

respectively (Fig. 4a). Besides, 51.6 % of the Eurasian drylands experienced a slight increase in MAP—particularly in EAS (3.40 mm yr^{-2}) and SAS (4.29 mm yr^{-2}), while 48.40 % of the area showed decrease in MAP (Fig. 4b). However, the spatial patterns of SM and TWS differed from those observed for MAP. Approximately 30.9 % and 49.6 % of the Eurasian drylands showed significant declines in SM and TWS, respectively, except for SM in EAS and CAS having increasing rates of 0.001 and $0.001 \text{ m}^3 \text{ m}^{-3} \text{ yr}^{-1}$, respectively (Fig. 4c and d). Although SAS showed an increase in MAP of 4.29 mm yr^{-2} , both SM and TWS in this subregion exhibited decreasing trends, with rates of $-0.001 \text{ m}^3 \text{ m}^{-3} \text{ yr}^{-1}$ and -0.75 mm yr^{-1} , respectively. Other than that, WAS, NAS, MED, and CNEU had consistent declines in both SM and TWS. Furthermore, 38.4 % of the Eurasian drylands experienced significant VPD increases during 2003–2020, with the highest and second-highest rises observed in WAS ($0.007 \text{ kPa yr}^{-1}$) and CNEU ($0.006 \text{ kPa yr}^{-1}$), respectively (Fig. 4e). Approximately 54.8 % of the Eurasian drylands showed a slight increase in SSRD, while TIB, EAS and SAS showed decreases in SSRD, with the rate of -0.67 , -1.09 , and $-4.31 \text{ W m}^{-2} \text{ yr}^{-1}$, respectively (Fig. 4f).

3.3. Effects of environmental factors on the temporal variability of vegetation in the Eurasian drylands

As shown in Fig. 2, CO_2 fertilization contributed to the overall vegetation greening in Eurasian drylands. The differences between LAI_{obs} and LAI_{adj} , GPP_{obs} , and GPP_{adj} quantifies the contributions of CO_2 fertilization on LAI and GPP. Accordingly, CO_2 fertilization accounted for 3.37 % and 2.59 % of increases in LAI and GPP, respectively, over the study period (Fig. S4). At the pixel scale, the spatial mean between the original satellite observations and the adjusted values was $0.02 \text{ m}^2 \text{ m}^{-2}$ and $7.79 \text{ g C m}^{-2} \text{ yr}^{-1}$, respectively. At the subregional scale, the contribution of the CO_2 fertilization effect to LAI and GPP was higher in the CNEU, MED, NAS, EAS, and SAS regions compared to other regions (Fig. S5). The CO_2 fertilization effect generally showed an increasing trend, with the lowest effect observed in CAS ($0.0002 \text{ m}^2 \text{ m}^{-2} \text{ yr}^{-1}$ and $0.64 \text{ g C m}^{-2} \text{ yr}^{-1}$) and TIB ($0.001 \text{ m}^2 \text{ m}^{-2} \text{ yr}^{-1}$ and $0.62 \text{ g C m}^{-2} \text{ yr}^{-1}$) compared to other regions (Fig. S6). Furthermore, after removing the CO_2 fertilization effects on satellite-observed LAI and GPP, the effects of environmental factors on the temporal variability of vegetation in the Eurasian drylands were evaluated. Our results revealed consistent

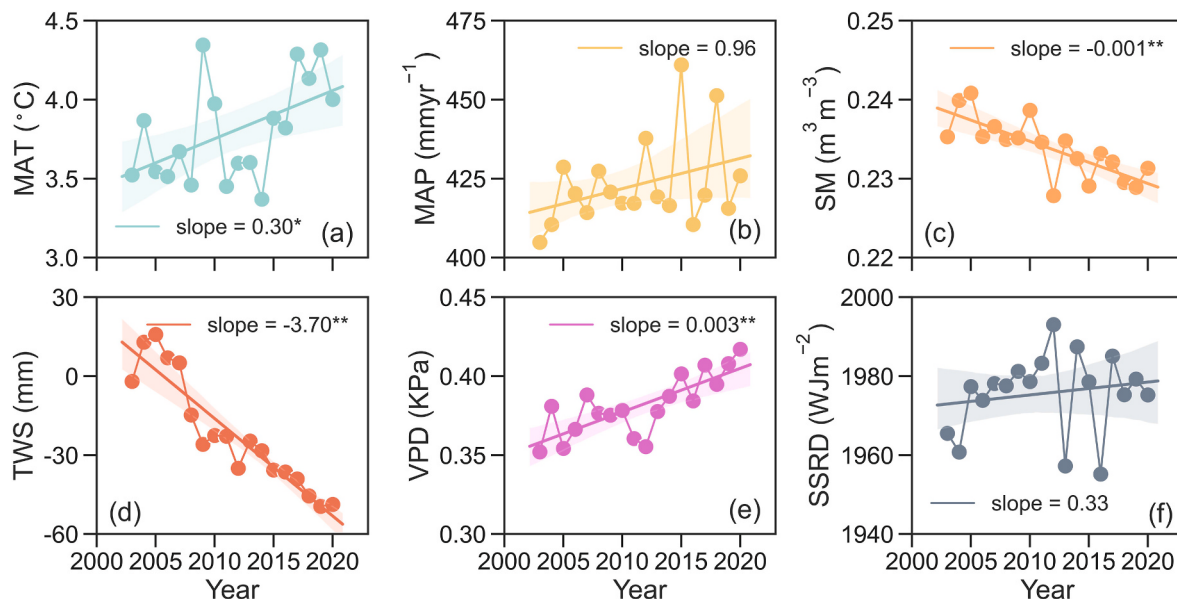


Fig. 3. The temporal trends of MAT (a), MAP (b), SM (c) TWS (d), VPD (e) and SSRD (f) in Eurasian drylands from 2003 to 2020. Note: the “*” and “**” indicates $p < 0.05$ and $p < 0.01$.

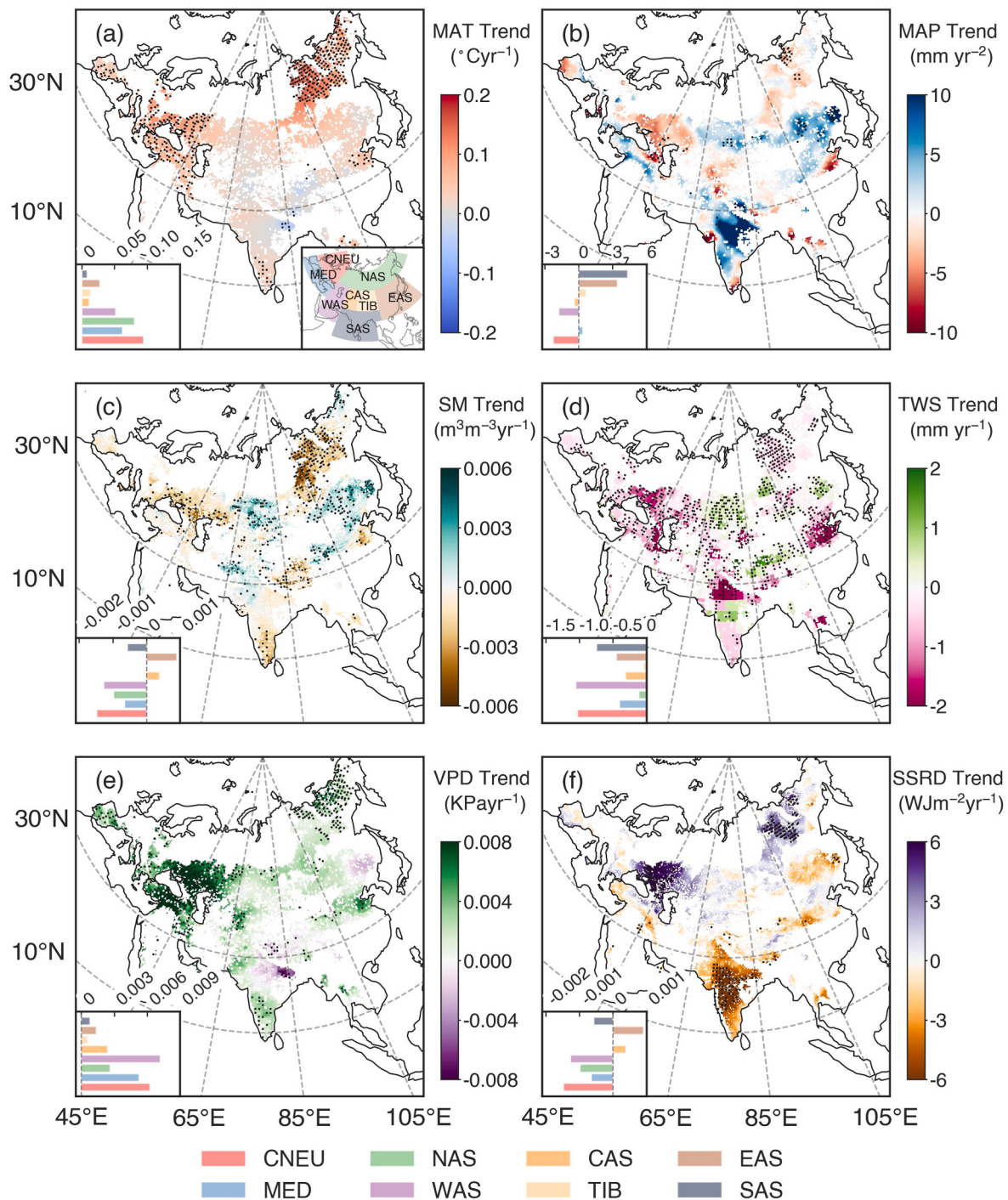


Fig. 4. The temporal trends of MAT (a), MAP (b), SM (c), TWS (d), VPD (e), and SSRD (f) in Eurasian drylands at pixel scale from 2003 to 2020. The colors of bars in inset charts indicate different regions as is shown in lower right of Fig. 4a. The statistically significant regions ($p < 0.05$) are labeled with black spots.

positive effects of MAT on the temporal variability of vegetation in the Eurasian drylands, which contributed to 58.71 % of LAI_{adj} and 64.58 % of GPP_{adj} of the Eurasian drylands, while a negative effect of MAT was found in the SAS for LAI_{adj} and GPP_{adj} (Fig. 5a and b). The contribution of MAP showed both positive and negative effects on the temporal variability of vegetation, which were roughly balanced across the Eurasian region (47.07 % vs. -45.98 % for LAI_{adj} and 44.10 % vs. -44.31 % for GPP_{adj}) (Fig. 5c and d). Moreover, SM had overall positive relationships with the temporal variability of vegetation across the Eurasian drylands (LAI_{adj} : 59.42 % and GPP_{adj} : 71.64 %) (Fig. 5e and f). For LAI_{adj} , TWS exhibited a positive relationship (47.84 %) across all

regions except NAS. In contrast, TWS showed a positive relationship (45.12 %) in most regions for GPP_{adj} except for CNEU and NAS. (Fig. 5g and h). VPD had negative effects on the temporal variability of vegetation in the Eurasian drylands (LAI_{adj} : 54.50 %; GPP_{adj} : 56.05 %) and a positive effect on the temporal variability of vegetation in CNEU and SAS for GPP_{adj} (Fig. 5i and j). The contribution of SSRD had both positive and negative effects on LAI_{adj} , and this effect was roughly balanced. However, the positive effect of GPP was greater than the negative effect (Fig. 5k and l). Overall, there was a widespread positive relationship between environmental factors (i.e. MAT, SM, and TWS) and temporal variability in vegetation across the entire Eurasian drylands.

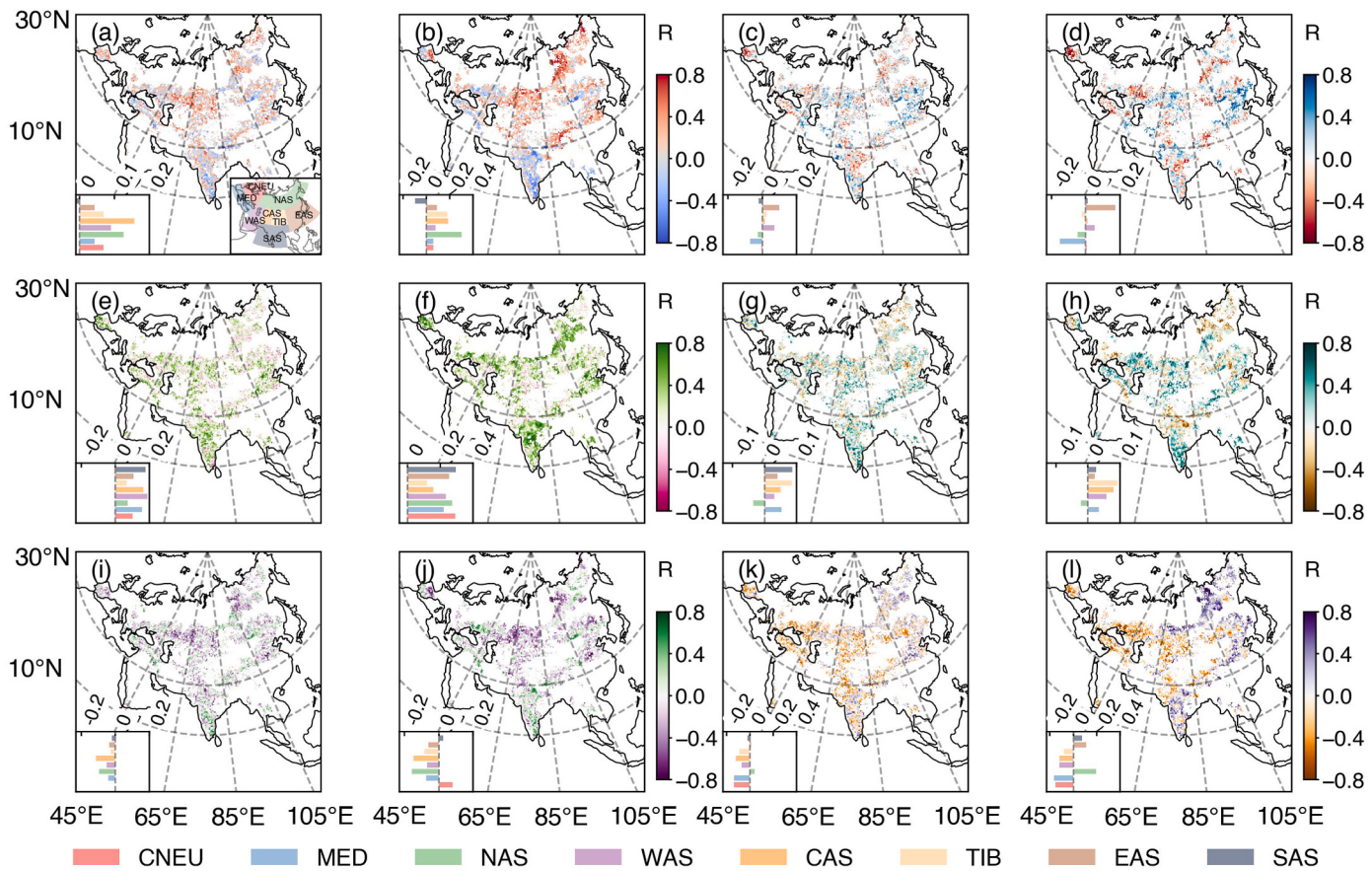


Fig. 5. Spatial patterns of partial correlation coefficient between vegetation dynamics (LAI_{adj} (a, c, e, g, i, and k) and GPP_{adj} (b, d, f, h, j, and l)) and environmental change (MAT (a, b), MAP (c, d), SM (e, f), TWS (g, h), VPD (i, j), and SSRD (k, l)). The colors of bars in inset charts indicate different regions as is shown in lower right of Fig. 5a.

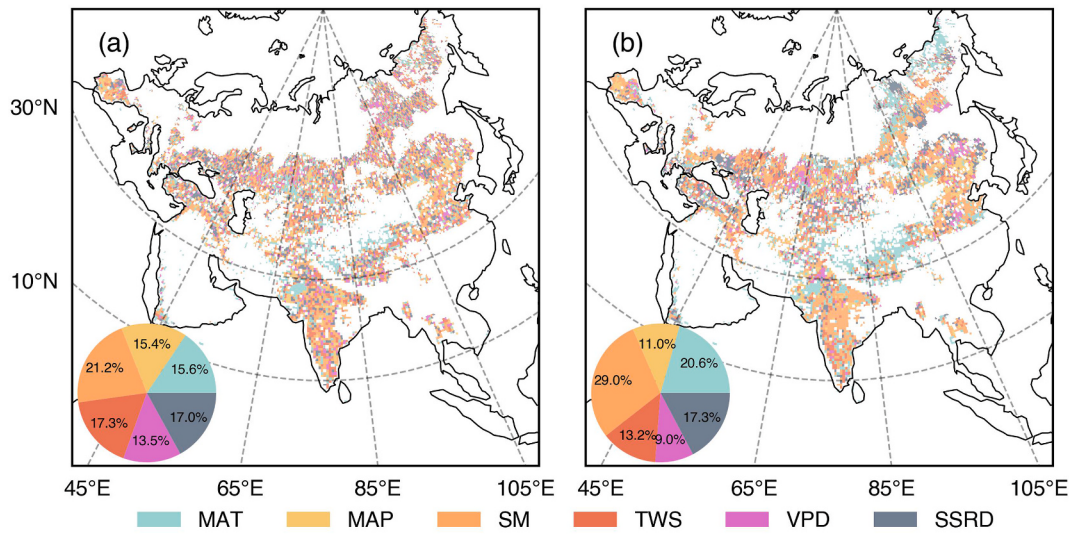


Fig. 6. Spatial patterns of dominant environmental variables on LAI_{adj} (a) and GPP_{adj} (b) from 2003 to 2020 in Eurasian drylands.

The dominant environmental variables were investigated to explore the roles of environmental variables in relation to the temporal variability of vegetation in the Eurasian drylands during 2003–2020. Results revealed large inconsistencies in the dominant environmental variables for different vegetation dynamic variables in the Eurasian drylands. SM dominated the temporal variabilities of LAI_{adj} and GPP_{adj} in most Eurasian drylands (21.2 % and 29.0 %, respectively) (Fig. 6a and b).

VPD had the lowest impacts on the temporal variability of vegetation (13.5 % and 9.0 %, respectively) compared with those of the other environmental factors. MAT dominated the temporal variability of vegetation (LAI_{adj} and GPP_{adj}), mainly in the high-altitude and high-latitude regions (e.g., Qinghai-Tibet Plateau and Northern Eurasian Drylands). MAP, TWS, and SSRD dominated the temporal variability of LAI_{adj} in most Eurasian drylands (15.4 %, 17.3 %, and 17.0 %,

respectively). The effect of SSRD (17.3 %) on the temporal variability of GPP_{adj} was greater than those of TWS and MAP (13.2 % and 11.0 %, respectively). Overall, the contribution of water availability (MAP, SM, and TWS) to the temporal variability of vegetation in the Eurasian drylands was greater than those of the MAT and SSRD.

3.4. Contributions of environmental factors and anthropogenic activities to vegetation greening

In general, both environmental variables and anthropogenic activities positively contributed to vegetation greening across the entire Eurasian drylands. However, anthropogenic activity more dominated vegetation greening, while the contributions of environmental factors show spatial variabilities (Fig. 7). The environmental factors in the Eurasian drylands contributed to slight increases in LAI_{adj} ($0.08 \text{ m}^2 \text{ m}^{-2} \text{ yr}^{-1}$) and GPP_{adj} ($0.05 \text{ g C m}^{-2} \text{ yr}^{-2}$) (Fig. 7a and b). The anthropogenic activities led to increasing vegetation growth over the Eurasian drylands, with $0.13 \text{ m}^2 \text{ m}^{-2} \text{ yr}^{-1}$ for LAI_{adj} and $0.13 \text{ g C m}^{-2} \text{ yr}^{-2}$ for GPP_{adj} (Fig. 7c and d).

Our results also consistently highlight the dominant role of anthropogenic activities in vegetation greening in both the Eurasian drylands as a whole and the eight subregions. The contributions of anthropogenic activities to vegetation greening (LAI_{adj} and GPP_{adj}) were positive in the subregions except in the case of CNEU ($-0.06 \text{ g C m}^{-2} \text{ yr}^{-2}$ for GPP_{adj}) (Fig. 7c and d). On the other hand, the contributions of environmental factors to the temporal variability of vegetation (LAI_{adj} and GPP_{adj}) were

not consistent in the eight subregions and the entire Eurasian drylands. The contributions of environmental variables to vegetation greening (LAI_{adj}) were positive except in the case of WAS ($-0.005 \text{ m}^2 \text{ m}^{-2} \text{ yr}^{-1}$). The contributions of environmental variables to vegetation greening (GPP_{adj}) were positive in CAS, NAS, MED, TIB, SAS, and EAS (0.008, 0.015, 0.070, 0.076, 0.077, and $0.265 \text{ g C m}^{-2} \text{ yr}^{-2}$).

4. Discussion

The analysis of vegetation dynamics and environmental changes in the Eurasian drylands from 2003 to 2020 provides a comprehensive understanding of the ecological response of vegetation to environmental variations in the region. Our findings showed significant increases in vegetation greenness and productivity, indicated by rising trends in LAI and GPP over the study period. Both observed and adjusted values of LAI (LAI_{obs} : 0.009, LAI_{adj} : $0.007 \text{ m}^2 \text{ m}^{-2} \text{ yr}^{-1}$) and GPP (GPP_{obs} : 2.08, GPP_{adj} : $1.06 \text{ C m}^{-2} \text{ yr}^{-2}$ for GPP_{obs}) consistently reflected this trend, underscoring the robustness of the greening signal. These results aligned with other remote sensing products (Zhang et al., 2024c) and land surface model simulations (Wang et al., 2023). Despite the overall greening, vegetation dynamics showed marked spatial variability, shaped by regional anthropogenic and environmental drivers. Notable greening occurred in Turkey, India, and northern and northeastern China (Li et al., 2021; Potapov et al., 2021). In Turkey and India, agricultural expansion, improved irrigation, and modern farming technologies were key drivers (Potapov et al., 2021). In northern China,

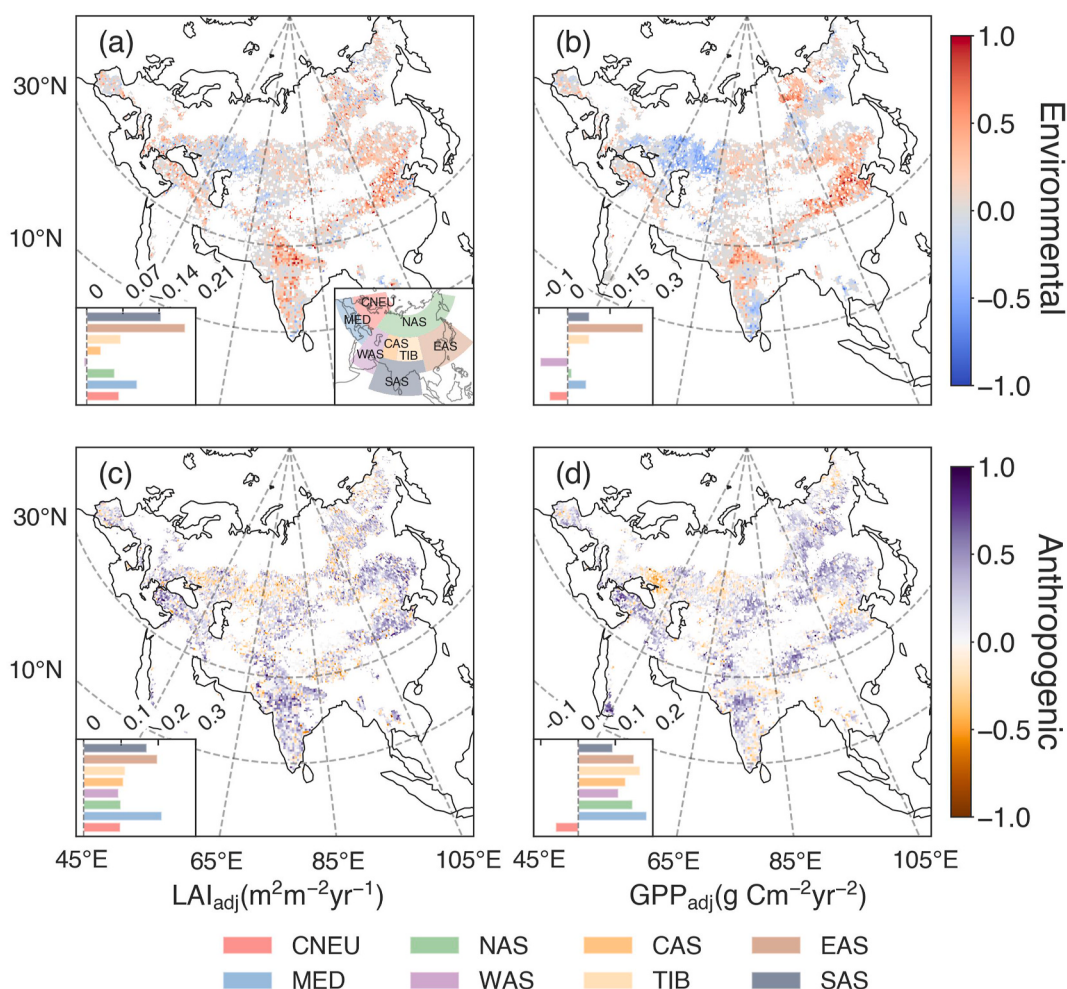


Fig. 7. The actual contribution of environmental changes and anthropogenic activities to vegetation dynamics (LAI_{adj} (a, c), GPP_{adj} (b, d)) at the pixel scale. The colors of bars in inset charts indicate different regions as is shown right of Fig. 7a.

large-scale afforestation programs aimed at controlling desertification and erosion played a central role (Li et al., 2021). In contrast, Central Asia experienced browning, largely due to land degradation from overgrazing, unsustainable farming, and wildfires (Hao et al., 2021; Lv et al., 2025).

The environmental conditions in Eurasian drylands have gone through relatively stable changes. We found that a large portion of the Eurasian drylands experienced a significant increase in MAT and a slight increase in MAP and SSRD during the study period (Figs. 3 and 4). These results are consistent with those of other reports on Asian drylands since the 1980s (Huang et al., 2017). However, a slight increase in MAP did not lead to an increase in SM or TWS, suggesting that evapotranspiration driven by warming temperatures may exacerbate water stress, even in areas with rising precipitation (Stark and Fridley, 2023). The significant decline in TWS was primarily observed in North China, India, and Western Central Asia in the Eurasian drylands (Figs. 3d and 4d). The excessive groundwater extraction for irrigation in North China and India resulted in the decline in TWS (Lai et al., 2022). In contrast, the decline in TWS in Western Central Asia was likely attributed to the reduction in SM (Jensen et al., 2024). Our results showed a significant increase in VPD (Figs. 3e and 4e), which could further elevate evapotranspiration, accelerating the depletion of water availability (SM and TWS). Consequently, the reduction in water availability also led to increase near-surface air temperature, further increasing VPD (Liu et al., 2023). This phenomenon was more pronounced in the Central Asia (Huang et al., 2021).

The CO₂ fertilization effect can be influenced by nutrients availability and environmental conditions (Terrer et al., 2019; Wang et al., 2020). Our results showed a generally increasing CO₂ fertilization effect on vegetation growth across Eurasian drylands, but the magnitude of this increase exhibited strong spatial heterogeneity (Fig. S5 and Fig. S6). In arid and semi-arid ecosystems, limited water availability imposes strong constraints on the physiological responsiveness of vegetation to elevated CO₂, particularly by restricting stomatal conductance and photosynthetic efficiency (Keenan et al., 2023; Li et al., 2023). In our results, the CO₂ fertilization effect was relatively high in India, China, and Turkey due to higher water availability (i.e., MAP, SM, and TWS), but much lower in Central Asia, where persistent moisture deficits likely suppressed the response (Fig. 4). In addition, the CO₂ fertilization effect is known to be constrained when plant growth is limited by nitrogen availability (Reich et al., 2014). Recent findings show that nitrogen availability has declined across large portions of the Eurasian drylands, particularly in Central Asia and parts of the Middle East, whereas increasing trends are observed in northeastern China and India (Fig. S6) (Mason et al., 2022). This spatial pattern aligns with our results, where regions exhibiting relatively stable or increasing nitrogen availability also show stronger CO₂ fertilization effects, suggesting that regional variability in nutrient trends plays an important role in modulating vegetation responses to elevated atmospheric CO₂. Moreover, our findings are consistent with recent studies suggesting that the global CO₂ fertilization effect has weakened in recent years. Specifically, the positive influence of atmospheric CO₂ on LAI and GPP slowed after 2015 (Fig. S4). This finding is consistent with previous work, which suggested that rising CO₂ levels may have limited impact on GPP sensitivity to soil moisture and vapor pressure deficit, potentially because CO₂ enrichment does not significantly alter whole-plant transpiration rates (Yu et al., 2024).

The observed greening trend aligns with previous studies linking CO₂ fertilization and improved water-use efficiency with vegetation recovery (Chen et al., 2024b). However, this study also reveals that positive vegetation trends persist even after excluding CO₂ fertilization, underscoring the significance of other factors like temperature and localized hydrological changes. Therefore, we assessed how vegetation dynamics responded to environmental changes (i.e. MAT, MAP, SM, TWS, VPD, and SSRD) using partial correlation analysis. Our results revealed predominantly positive correlations between MAT and vegetation variables

in most of the Eurasian regions. These positive correlations can be attributed to the cold and humid climate in high-latitude and high-altitude regions, where vegetation growth is primarily constrained by temperature or solar radiation (Ge et al., 2021). On the one hand, warming increases the amount of water available from glaciers and snowmelt for vegetation growth (Teng et al., 2020). It also extends the growing season and significantly enhances vegetation greenness and productivity, particularly in high-latitude and high-altitude regions (Chen et al., 2024b). Additionally, warming can lead to increased evapotranspiration and SM deficits, leading to weakened vegetation productivity from a long-term perspective (Gampe et al., 2021). Furthermore, previous studies demonstrated that water availability is a limiting factor for vegetation growth in drylands (Liu et al., 2023). Ukkola et al. (2021) and Walther et al. (2018) showed that the temporal trend of MAP across drylands has a limited ability to explain vegetation dynamics. This is consistent with our findings showing a positive correlation between water availability (SM and TWS) and vegetation greening across a broader range of the Eurasian drylands. SM and TWS partly explain water availability in the Eurasian drylands. In our results, SM emerges as the predominant factor influencing temporal variability of vegetation in a substantial proportion of the Eurasian drylands, irrespective of the specific vegetation data employed. This is because MAP and TWS can only provide indirect information on the surface water conditions, whereas SM can be directly utilized by vegetation (Liu et al., 2023; Yu et al., 2024). In addition, our results indicate that the Eurasian drylands have become greener and more productive, albeit with an elevated VPD, which is consistent with the results from Liu et al. (2023) and Chen et al. (2024b). This phenomenon is likely due to the warming and the CO₂ fertilization effect (Song et al., 2022). Our study indicated that the correlation of LAI_{adj} (GPP_{adj}) with MAP is positive and those with VPD are negative in most regions, high VPD combined with higher MAT promotes vegetation growth in colder or high altitude regions (Yu et al., 2024).

The impacts of anthropogenic activities on the Eurasian drylands ecosystems have notably emerged. Our results indicate a positive dominant impact of anthropogenic activities on vegetation greening in the Eurasian drylands, which is a consequence of combined effects of positive (e.g., afforestation, land management, irrigation) and negative effects (e.g., land-use change) of anthropogenic activities. On the one hand, vegetation greening can be attributed to afforestation (Qu et al., 2020; Yuan et al., 2021) and cropland expansion (Potapov et al., 2021), which is consistent with our findings (Fig. 2). Human activities contributed 66 % of the increase in vegetation greenness in the agro-pastoral ecotone of northern China (Pei et al. (2021)). In Northwest India, large areas of barren land were converted into shrublands, and then converted into croplands after the Green Revolution, potentially contributing to greening (Prijith et al. (2021)). On the other hand, land-use change, such as urban expansion, and other human activities, such as overgrazing and industrial activities disrupt existing vegetation growth and distribution, leading to negative impacts on vegetation dynamics in Eurasian drylands (Hao et al., 2021).

Although our results indicate that both environmental variables and anthropogenic activities contribute positively to vegetation greening, climate models projected an increasing aridity in the Eurasian drylands (Lian et al., 2021). Consequently, the positive contribution of environmental factors to vegetation greening may decline in the future, potentially resulting in a trend of vegetation browning. Moreover, numerous studies have confirmed that revegetation in dryland is approaching sustainable water resource limits (Liu et al., 2023). Failure to adjust vegetation planting strategies according to local water availability may lead to excessive depletion of local water resources and deterioration of the ecological environment (Huang et al., 2021). Future climate change was projected to weaken the CO₂ fertilization effect, particularly in arid and semi-arid regions where vegetation growth was already limited by water and nutrient availability. With increasing aridity, the physiological advantages conferred by elevated atmospheric

CO₂ concentrations were likely offset by intensified environmental stress, thereby introducing substantial uncertainty into future vegetation dynamics. Therefore, the greening trends observed in the past were unlikely to persist under future climate scenarios, especially in the absence of adaptive land management practices. Future research is thus needed to better quantify how changes in CO₂ concentrations, environmental constraints, and anthropogenic activities further influence vegetation trajectories under different climate scenarios.

Moreover, to enhance the credibility of our findings, we conducted a supplementary analysis using independent satellite-derived datasets, specifically GIMMS LAI and BESS GPP. These alternative datasets provided an independent and complementary perspective on vegetation structure and productivity across the Eurasian drylands. The results obtained from this reanalysis exhibited spatial and temporal patterns that were broadly consistent with those derived from our original datasets, thereby reinforcing the robustness of the identified CO₂ fertilization effect and its contribution to vegetation dynamics (Fig. S7–S13). This cross-validation strengthened the validity of our conclusions and mitigated uncertainties associated with the reliance on a single data source.

Although our study analyzes the impacts of multiple environmental variables and anthropogenic activities on vegetation dynamics, several limitations remain. Our analysis did not account for indirect anthropogenic activities such as air pollution, which can significantly impact vegetation health and growth. Air pollutants, including ozone and particulate matter, have been documented to affect photosynthesis rates and overall plant productivity (Hashad et al., 2023; Molnár et al., 2020). Future research should incorporate these factors to better understand and quantify the true extent of CO₂ fertilization effects and anthropogenic activities on vegetation dynamics in the Eurasian drylands.

5. Conclusion

The Eurasian drylands have experienced vegetation greening over the past two decades due to both environmental changes and anthropogenic activities. However, the underlying driving factors behind these influences remain unclear for the region. This study conducted a contribution analysis to quantify the impacts of environmental changes and anthropogenic activities on vegetation dynamics across the Eurasian drylands from 2003 to 2020. By using the satellite-observed datasets, our results revealed significant increasing trends in both vegetation greenness and productivity during the study period. CO₂ fertilization effect accounted for 3.37 % and 2.59 % of the increase, while water availability, among the environmental factors characterized by distinct spatial-temporal changing patterns, was attributed to more than 50 % of the increase irrespective of the CO₂ fertilization. Besides, the net effects of anthropogenic activities resulted in greater increases in vegetation dynamics than those attributable to environmental changes. Practices such as cropland expansion, ecological conservation, and restoration have been the primary drivers of greening in Eurasian drylands, particularly in hotspot regions like China and India. Our findings clarify the distinct effects of environmental changes and anthropogenic activities on vegetation greening in Eurasian drylands, underscoring their significance for ecological management and sustainable development in the context of future climate change.

CRediT authorship contribution statement

Jinyue Liu: Writing – original draft, Software, Investigation, Data curation. **Chao Yue:** Supervision, Resources, Project administration, Methodology, Funding acquisition, Conceptualization. **Fan Yi:** Investigation. **Pengyi Zhang:** Writing – review & editing, Validation. **Junhao He:** Writing – review & editing, Methodology, Formal analysis. **Jie Zhao:** Visualization.

Declaration of competing interest

The authors declare that they have no known competing financial interests or personal relationships that could have appeared to influence the work reported in this paper.

Acknowledgments

We thank the TRENDY DGVM community and all people and institutions who provided these datasets used in this study. This study was supported by the National Key Research and Development Program of China (2023YFB3907403), the Second Tibetan Plateau Scientific Expedition and Research Program (2022QZKK0101), the National Natural Science Foundation of China (U20A2090, 41971132), and the Strategic Priority Research Program of the Chinese Academy of Sciences (XDB40000000). C.Y. acknowledges the support from Open-end Funds of Ministry of Education Key Laboratory for Earth System Modeling (Tsinghua University).

Appendix A. Supplementary data

Supplementary data to this article can be found online at <https://doi.org/10.1016/j.jenvman.2025.126604>.

Data availability

The aridity index dataset is from https://figshare.com/articles/dataset/Global_Aridity_Index_and_Potential_Evapotranspiration_ET0_Climate_Database_v2/7504448/3?file=13901336. The ESA-CCI land cover dataset is available at <https://cds.climate.copernicus.eu/cdsapp#!/dataset/satellite-land-cover?tab=form>. The spatial boundaries of 8 regions used in this study are from the IPCC SREX report (https://www.ipcc-data.org/guidelines/pages/ar5_regions.html). The satellite observation datasets used in this study are available at <https://lpdaac.usgs.gov/>. The TRENDY v.10 datasets applied in this study were requested from S. Sitch (s.a.sitch@exeter.ac.uk) and P. Friedlingstein (p.friedlingstein@exeter.ac.uk). Mean annual temperature, mean annual precipitation, maximum and minimum air temperatures, and actual vapor pressure datasets can be obtained at <https://crudata.uea.ac.uk/cru/data/hrg/>. The soil moisture dataset is from <https://disc.gsfc.nasa.gov/>. The terrestrial water storage dataset can be obtained at <https://podaac.jpl.nasa.gov/cloud-datasets>. Surface solar radiation downwards datasets is from <https://cds.climate.copernicus.eu/cdsapp#!/dataset/reanalysis-era5-land-monthly-means?tab=overview>.

References

- Bai, Q., Wang, T., Han, Q., Li, X., 2025. Vegetation dynamics induced by climate change and human activities: implications for coastal wetland restoration. *J. Environ. Manag.* 384, 125594. <https://doi.org/10.1016/j.jenvman.2025.125594>.
- Banerjee, A., Kang, S., Meadows, M.E., Xia, Z., Sengupta, D., Kumar, V., 2023. Quantifying climate variability and regional anthropogenic influence on vegetation dynamics in northwest India. *Environ. Res.* 234, 116541. <https://doi.org/10.1016/j.enres.2023.116541>.
- Burrell, A.L., Evans, J.P., De Kauwe, M.G., 2020. Anthropogenic climate change has driven over 5 million km(2) of drylands towards desertification. *Nat. Commun.* 11, 3853. <https://doi.org/10.1038/s41467-020-17710-7>.
- Chen, J., Yang, H., Jin, T., Wu, K., 2024a. Assessment of terrestrial ecosystem sensitivity to climate change in arid, semi-arid, sub-humid, and humid regions using EVI, LAI, and SIF products. *Ecol. Indic.* 158, 111511. <https://doi.org/10.1016/j.ecolind.2023.111511>.
- Chen, Z., Wang, W., Forzieri, G., Cescatti, A., 2024b. Transition from positive to negative indirect CO(2) effects on the vegetation carbon uptake. *Nat. Commun.* 15, 1500. <https://doi.org/10.1038/s41467-024-45957-x>.
- Deng, H., Chen, Y., 2017. Influences of recent climate change and human activities on water storage variations in central Asia. *J. Hydrol.* 544, 46–57. <https://doi.org/10.1016/j.jhydrol.2016.11.006>.
- Ding, Z., Peng, J., Qiu, S., Zhao, Y., 2020. Nearly half of global vegetated area experienced inconsistent vegetation growth in terms of greenness, cover, and productivity. *Earths Future* 8. <https://doi.org/10.1029/2020ef001618>.

- Feng, X., Fu, B., Piao, S., Wang, S., Ciais, P., Zeng, Z., Lü, Y., Zeng, Y., Li, Y., Jiang, X., 2016. Revegetation in China's Loess Plateau is approaching sustainable water resource limits. *Nat. Clim. Change* 6, 1019–1022. <https://doi.org/10.1038/nclimate3092>.
- Field, C.B., Barros, V., Stocker, T.F., Dahe, Q., 2012. *Managing the Risks of Extreme Events and Disasters to Advance Climate Change Adaptation: Special Report of the Intergovernmental Panel on Climate Change*. Cambridge University Press.
- Franks, P.J., Adams, M.A., Amthor, J.S., Barbour, M.M., Berry, J.A., Ellsworth, D.S., Farquhar, G.D., Ghannoum, O., Lloyd, J., McDowell, N., Norby, R.J., Tissue, D.T., von Caemmerer, S., 2013. Sensitivity of plants to changing atmospheric CO₂ concentration: from the geological past to the next century. *New Phytol.* 197, 1077–1094. <https://doi.org/10.1111/nph.12104>.
- Fu, B., Stafford-Smith, M., Wang, Y., Wu, B., Yu, X., Lv, N., Ojima, D.S., Lv, Y., Fu, C., Liu, Y., Niu, S., Zhang, Y., Zeng, H., Liu, Y., Liu, Y., Feng, X., Zhang, L., Wei, Y., Xu, Z., Li, F., Cui, X., Diop, S., Chen, X., 2021. The Global-DEP conceptual framework — research on dryland ecosystems to promote sustainability. *Curr. Opin. Environ. Sustain.* 48, 17–28. <https://doi.org/10.1016/j.cosust.2020.08.009>.
- Gampe, D., Zscheischler, J., Reichstein, M., O'Sullivan, M., Smith, W.K., Sitch, S., Buermann, W., 2021. Increasing impact of warm droughts on northern ecosystem productivity over recent decades. *Nat. Clim. Change* 11, 772–779. <https://doi.org/10.1038/s41558-021-01112-8>.
- Ge, W., Deng, L., Wang, F., Han, J., 2021. Quantifying the contributions of human activities and climate change to vegetation net primary productivity dynamics in China from 2001 to 2016. *Sci. Total Environ.* 773, 145648. <https://doi.org/10.1016/j.scitotenv.2021.145648>.
- Guo, H., Tian, Y., Li, J., Meng, X., Lv, X., Wang, W., Bao, A., Zhu, L., Nzabarinda, V., De Maeyer, P., 2024. Unveiling the spatiotemporal impacts of the 2021 Central Asian drought on vegetation: a comprehensive quantitative analysis. *Ecol. Indic.* 165, 112238. <https://doi.org/10.1016/j.ecolind.2024.112238>.
- Hao, W.M., Reeves, M.C., Baggett, L.S., Balkanski, Y., Ciais, P., Nordgren, B.L., Petkov, A., Corley, R.E., Mouillet, F., Urbanski, S.P., Yue, C., 2021. Wetter environment and increased grazing reduced the area burned in northern Eurasia from 2002 to 2016. *Biogeosciences* 18, 2559–2572. <https://doi.org/10.5194/bg-18-2559-2021>.
- Harris, I., Osborn, T.J., Jones, P., Lister, D., 2020. Version 4 of the CRU TS monthly high-resolution gridded multivariate climate dataset. *Sci. Data* 7, 109. <https://doi.org/10.1038/s41597-020-0453-3>.
- Hashad, K., Yang, B., Gallagher, J., Baldauf, R., Deshmukh, P., Zhang, K.M., 2023. Impact of roadside conifers vegetation growth on air pollution mitigation. *Landsc. Urban Plann.* 229, 104594. <https://doi.org/10.1016/j.landurbplan.2022.104594>.
- Hu, F., Liang, B., Yang, G., Lu, Z., Li, Z., Fu, Y., 2025. Evaluation of groundwater storage variability and relationship with hydrometeoreological factors in the huang-huai-hai Plain, China, using GRACE and GLDAS Data (2002–2023). *J. Hydrol.: Reg. Stud.* 60, 102540. <https://doi.org/10.1016/j.ejrh.2025.102540>.
- Huang, J., Li, Y., Fu, C., Chen, F., Fu, Q., Dai, A., Shinoda, M., Ma, Z., Guo, W., Li, Z., Zhang, L., Liu, Y., Yu, H., He, Y., Xie, Y., Guan, X., Ji, M., Lin, L., Wang, S., Yan, H., Wang, G., 2017. Dryland climate change: recent progress and challenges. *Rev. Geophys.* 55, 719–778. <https://doi.org/10.1002/2016rg000550>.
- Huang, W., Duan, W., Chen, Y., 2021. Rapidly declining surface and terrestrial water resources in Central Asia driven by socio-economic and climatic changes. *Sci. Total Environ.* 784, 147193. <https://doi.org/10.1016/j.scitotenv.2021.147193>.
- Jensen, L., Gerdener, H., Eicker, A., Kusche, J., Fiedler, S., 2024. Observations indicate regionally misleading wetting and drying trends in CMIP6. *npj Climate Atmos. Sci.* 7, <https://doi.org/10.1038/s41612-024-00788-x>.
- Jiao, W., Wang, L., Smith, W.K., Chang, Q., Wang, H., D'Odorico, P., 2021. Observed increasing water constraint on vegetation growth over the last three decades. *Nat. Commun.* 12, 3777. <https://doi.org/10.1038/s41467-021-24016-9>.
- Keenan, T.F., Luo, X., Stocker, B.D., De Kauwe, M.G., Medlyn, B.E., Prentice, I.C., Smith, N.G., Terrer, C., Wang, H., Zhang, Y., Zhou, S., 2023. A constraint on historic growth in global photosynthesis due to rising CO₂. *Nat. Clim. Change* 13, 1376–1381. <https://doi.org/10.1038/s41558-023-01867-2>.
- Lai, J., Li, Y., Chen, J., Niu, G.-Y., Lin, P., Li, Q., Wang, L., Han, J., Luo, Z., Sun, Y., 2022. Massive crop expansion threatens agriculture and water sustainability in northwestern China. *Environ. Res. Lett.* 17, 034003. <https://doi.org/10.1088/1748-9326/ac46e8>.
- Landerer, F.W., Flechtner, F.M., Save, H., Webb, F.H., Bandikova, T., Bertiger, W.I., Bettadpur, S.V., Byun, S.H., Dahle, C., Dobslaw, H., Fahnestock, E., Harvey, N., Kang, Z., Kruizinga, G.L.H., Loomis, B.D., McCullough, C., Murböck, M., Nagel, P., Paik, M., Pie, N., Poole, S., Strelakov, D., Tamisiea, M.E., Wang, F., Watkins, M.M., Wen, H.Y., Wiese, D.N., Yuan, D.N., 2020. Extending the global mass change data record: GRACE follow-on instrument and science data performance. *Geophys. Res. Lett.* 47, <https://doi.org/10.1029/2020GL088306>.
- Li, C., Fu, B., Wang, S., Stringer, L.C., Wang, Y., Li, Z., Liu, Y., Zhou, W., 2021. Drivers and impacts of changes in China's drylands. *Nat. Rev. Earth Environ.* 2, 858–873. <https://doi.org/10.1038/s43017-021-00226-z>.
- Li, S., Wang, G., Zhu, C., Lu, J., Ullah, W., Fififi Tawia Hagan, D., Kattel, G., Liu, Y., Zhang, Z., Song, Y., Sun, S., Zheng, Y., Peng, J., 2023. Vegetation growth due to CO₂ fertilization is threatened by increasing vapor pressure deficit. *J. Hydrol.* 619, 129292. <https://doi.org/10.1016/j.jhydrol.2023.129292>.
- Li, Z., Chen, Y., Li, W., Deng, H., Fang, G., 2015. Potential impacts of climate change on vegetation dynamics in Central Asia. *J. Geophys. Res. Atmos.* 120, 12345–12356. <https://doi.org/10.1002/2015jd023618>.
- Lian, X., Piao, S., Chen, A., Huntingford, C., Fu, B., Li, L.Z.X., Huang, J., Sheffield, J., Berg, A.M., Keenan, T.F., McVicar, T.R., Wada, Y., Wang, X., Wang, T., Yang, Y., Roderick, M.L., 2021. Multifaceted characteristics of dryland aridity changes in a warming world. *Nat. Rev. Earth Environ.* 2, 232–250. <https://doi.org/10.1038/s43017-021-00144-0>.
- Liu, H., Liu, Y., Chen, Y., Fan, M., Chen, Y., Gang, C., You, Y., Wang, Z., 2023. Dynamics of global dryland vegetation were more sensitive to soil moisture: evidence from multiple vegetation indices. *Agric. For. Meteorol.* 331, 109327. <https://doi.org/10.1016/j.agrformet.2023.109327>.
- Liu, Y., Li, Y., Li, S., Motesharrei, S., 2015. Spatial and temporal patterns of global NDVI trends: correlations with climate and human factors. *Remote Sens.* 7, 13233–13250. <https://doi.org/10.3390/rs7101323>.
- Liu, Y., Liu, H., Chen, Y., Gang, C., Shen, Y., 2022. Quantifying the contributions of climate change and human activities to vegetation dynamic in China based on multiple indices. *Sci. Total Environ.* 838, 156553. <https://doi.org/10.1016/j.scitotenv.2022.156553>.
- Lv, Z., Li, S., Xu, X., Lei, J., Peng, Z., 2025. Assessment of vegetation restoration potential in central Asia. *J. Environ. Manag.* 374, 124089. <https://doi.org/10.1016/j.jenvman.2025.124089>.
- Maestre, F.T., Benito, B.M., Berdugo, M., Concostrina-Zubiri, L., Delgado-Baquerizo, M., Eldridge, D.J., Guirado, E., Gross, N., Kéfi, S., Le Bagousse-Pinguet, Y., 2021. Biogeography of global drylands. *New Phytol.* 231, 540–558. <https://doi.org/10.1111/nph.17395>.
- Mason, R.E., Craine, J.M., Lany, N.K., Jonard, M., Ollinger, S.V., Groffman, P.M., Fulweiler, R.W., Angerer, J., Read, Q.D., Reich, P.B., 2022. Evidence, causes, and consequences of declining nitrogen availability in terrestrial ecosystems. *Science* 376, eab3767. <https://doi.org/10.1126/science.abh3767>.
- Molnár, V.É., Simon, E., Tóthmérész, B., Ninsawat, S., Szabó, S., 2020. Air pollution induced vegetation stress – the air pollution tolerance index as a quick tool for city health evaluation. *Ecol. Indic.* 113, 106234. <https://doi.org/10.1016/j.ecolind.2020.106234>.
- Muñoz-Sabater, J., Dutra, E., Agustí-Panareda, A., Albergel, C., Arduini, G., Balsamo, G., Boussetta, S., Choulga, M., Harrigan, S., Hersbach, H., Martens, B., Miralles, D.G., Piles, M., Rodríguez-Fernández, N.J., Zsoter, E., Buontempo, C., Thépaut, J.-N., 2021. ERA5-Land: a state-of-the-art global reanalysis dataset for land applications. *Earth Syst. Sci. Data* 13, 4349–4383. <https://doi.org/10.5194/essd-13-4349-2021>.
- Mynevi, R., Knayazikhin, Y., Park, T., 2021. MODIS/terra leaf area index/FPAR 8-day L4 global 500m SIN grid V061. NASA EOSDIS Land Process. DAAC V061. <https://doi.org/10.5067/MODIS/MOD15A2H.061> [data set].
- Park, T., Gumma, M.K., Wang, W., Panjala, P., Dubey, S.K., Nemani, R.R., 2023. Greening of human-dominated ecosystems in India. *Commun. Earth Environ.* 4, 419. <https://doi.org/10.1038/s43247-023-01078-9>.
- Pei, H., Liu, M., Jia, Y., Zhang, H., Li, Y., Xiao, Y., 2021. The trend of vegetation greening and its drivers in the Agro-pastoral ecotone of northern China, 2000–2020. *Ecol. Indic.* 129, 108004. <https://doi.org/10.1016/j.ecolind.2021.108004>.
- Potapov, P., Turubanova, S., Hansen, M.C., Tyukavina, A., Zelles, V., Khan, A., Song, X.-P., Pickens, A., Shen, Q., Cortez, J., 2021. Global maps of cropland extent and change show accelerated cropland expansion in the twenty-first century. *Nat. Food* 3, 19–28. <https://doi.org/10.1038/s43016-021-00429-z>.
- Prijith, S.S., Srinivasarao, K., Lima, C.B., Gharai, B., Rao, P.V.N., SeshaSai, M.V.R., Ramana, M.V., 2021. Effects of land use/land cover alterations on regional meteorology over Northwest India. *Sci. Total Environ.* 765, 142678. <https://doi.org/10.1016/j.scitotenv.2020.142678>.
- Qu, S., Wang, L., Lin, A., Yu, D., Yuan, M., Li, C.a., 2020. Distinguishing the impacts of climate change and anthropogenic factors on vegetation dynamics in the Yangtze River Basin, China. *Ecol. Indic.* 108, 105724. <https://doi.org/10.1016/j.ecolind.2019.105724>.
- Reich, P.B., Hobbie, S.E., Lee, T.D., 2014. Plant growth enhancement by elevated CO₂ eliminated by joint water and nitrogen limitation. *Nat. Geosci.* 7, 920–924. <https://doi.org/10.1038/ngeo2284>.
- Reichgelt, T., D'Andrea, W.J., 2019. Plant carbon assimilation rates in atmospheric CO₂ reconstructions. *New Phytol.* 223, 1844–1855. <https://doi.org/10.1111/nph.15914>.
- Rodell, M., Houser, P., Jambor, U., Gottschalck, J., Mitchell, K., Meng, C.-J., Arsenault, K., Cosgrove, B., Radakovitch, J., Bosilovich, M., 2004. The global land data assimilation system. *Bull. Am. Meteorol. Soc.* 85, 381–394. <https://doi.org/10.1175/BAMS-85-3-381>.
- Running, S., Mu, Q., Zhao, M., 2021. MODIS/Terra gross primary productivity gap-filled 8-Day L4 global 500m SIN grid V061. NASA EOSDIS Land Process. Distribute. Active Arch. Center V061. <https://doi.org/10.5067/MODIS/MOD17A2HGF.061> [data set].
- Shi, S., Yu, J., Wang, F., Wang, P., Zhang, Y., Jin, K., 2021. Quantitative contributions of climate change and human activities to vegetation changes over multiple time scales on the Loess Plateau. *Sci. Total Environ.* 755, 142419. <https://doi.org/10.1016/j.scitotenv.2020.142419>.
- Song, Y., Jiao, W., Wang, J., Wang, L., 2022. Increased global vegetation productivity despite rising atmospheric dryness over the last two decades. *Earths Future* 10. <https://doi.org/10.1029/2021ef002634>.
- Stark, J.R., Fridley, J.D., 2023. Topographic drivers of soil moisture across a large sensor network in the Southern Appalachian Mountains (USA). *Water Resour. Res.* 59, e2022WR034315. <https://doi.org/10.1029/2022WR034315>.
- Teng, M., Zeng, L., Hu, W., Wang, P., Yan, Z., He, W., Zhang, Y., Huang, Z., Xiao, W., 2020. The impacts of climate changes and human activities on net primary productivity vary across an ecotone zone in Northwest China. *Sci. Total Environ.* 714, 136691. <https://doi.org/10.1016/j.scitotenv.2020.136691>.
- Terrer, C., Jackson, R.B., Prentice, I.C., Keenan, T.F., Kaiser, C., Vicca, S., Fisher, J.B., Reich, P.B., Stocker, B.D., Hungate, B.A., Penuelas, J., McCallum, I., Soudzilovskaya, N.A., Cernusak, L.A., Talhelm, A.F., Van Sundert, K., Piao, S., Newton, P.C.D., Hovenden, M.J., Blumenthal, D.M., Liu, Y.Y., Müller, C., Winter, K., Field, C.B., Viechtbauer, W., Van Lissa, C.J., Hoosbeek, M.R., Watanabe, M.,

- Koike, T., Leshyk, V.O., Polley, H.W., Franklin, O., 2019. Nitrogen and phosphorus constrain the CO₂ fertilization of global plant biomass. *Nat. Clim. Change* 9, 684–689. <https://doi.org/10.1038/s41558-019-0545-2>.
- Tian, F., Zhu, Z., Cao, S., Zhao, W., Li, M., Wu, J., 2024. Satellite-observed increasing coupling between vegetation productivity and greenness in the semiarid Loess Plateau of China is not captured by process-based models. *Sci. Total Environ.* 906, 167664. <https://doi.org/10.1016/j.scitotenv.2023.167664>.
- Ukkola, A.M., De Kauwe, M.G., Roderick, M.L., Burrell, A., Lehmann, P., Pitman, A.J., 2021. Annual precipitation explains variability in dryland vegetation greenness globally but not locally. *Glob. Change Biol.* 27, 4367–4380. <https://doi.org/10.1111/gcb.15729>.
- Venkatesh, K., John, R., Chen, J., Xiao, J., Amirkhiz, R.G., Giannico, V., Kussainova, M., 2022. Optimal ranges of social-environmental drivers and their impacts on vegetation dynamics in Kazakhstan. *Sci. Total Environ.* 847, 157562. <https://doi.org/10.1016/j.scitotenv.2022.157562>.
- Walther, S., Guanter, L., Heim, B., Jung, M., Duveiller, G., Wolanin, A., Sachs, T., 2018. Assessing the dynamics of vegetation productivity in circumpolar regions with different satellite indicators of greenness and photosynthesis. *Biogeosciences* 15, 6221–6256. <https://doi.org/10.5194/bg-15-6221-2018>.
- Wang, H., Yan, S., Ciais, P., Wigneron, J.P., Liu, L., Li, Y., Fu, Z., Ma, H., Liang, Z., Wei, F., Wang, Y., Li, S., 2022. Exploring complex water stress-gross primary production relationships: impact of climatic drivers, main effects, and interactive effects. *Glob. Change Biol.* 28, 4110–4123. <https://doi.org/10.1111/gcb.16201>.
- Wang, S., Fu, B., Wei, F., Piao, S., Maestre, F.T., Wang, L., Jiao, W., Liu, Y., Li, Y., Li, C., Zhao, W., 2023. Drylands contribute disproportionately to observed global productivity increases. *Sci Bull (Beijing)* 68, 224–232. <https://doi.org/10.1016/j.scib.2023.01.014>.
- Wang, S., Zhang, Y., Ju, W., Chen, J.M., Ciais, P., Cescatti, A., Sardans, J., Janssens, I.A., Wu, M., Berry, J.A., 2020. Recent global decline of CO₂ fertilization effects on vegetation photosynthesis. *Science* 370, 1295–1300. <https://doi.org/10.1126/science.abb7772>.
- Watkins, M.M., Wiese, D.N., Yuan, D.N., Boening, C., Landerer, F.W., 2015. Improved methods for observing Earth's time variable mass distribution with GRACE using spherical cap mascons. *J. Geophys. Res. Solid Earth* 120, 2648–2671. <https://doi.org/10.1002/2014jb011547>.
- Wu, J., Li, M., Zhang, X., Fiedler, S., Gao, Q., Zhou, Y., Cao, W., Hassan, W., Margarint, M.C., Tarolli, P., Tietjen, B., 2021. Disentangling climatic and anthropogenic contributions to nonlinear dynamics of alpine grassland productivity on the Qinghai-Tibetan Plateau. *J. Environ. Manag.* 281, 111875. <https://doi.org/10.1016/j.jenvman.2020.111875>.
- Wu, K., Ryu, D., Wagner, W., Hu, Z., 2023. A global-scale intercomparison of Triple collocation analysis- and ground-based soil moisture time-variant errors derived from different rescaling techniques. *Remote Sens. Environ.* 285, 113387. <https://doi.org/10.1016/j.rse.2022.113387>.
- Xie, S., Mo, X., Hu, S., Liu, S., 2020. Contributions of climate change, elevated atmospheric CO₂ and human activities to ET and GPP trends in the Three-North Region of China. *Agric. For. Meteorol.* 295, 108183. <https://doi.org/10.1016/j.agrformet.2020.108183>.
- Yang, R., Wang, J., Zeng, N., Sitch, S., Tang, W., McGrath, M.J., Cai, Q., Liu, D., Lombardozzi, D., Tian, H., Jain, A.K., Han, P., 2022. Divergent historical GPP trends among state-of-the-art multi-model simulations and satellite-based products. *Earth Syst. Dyn.* 13, 833–849. <https://doi.org/10.5194/esd-13-833-2022>.
- Yao, J., Liu, H., Huang, J., Gao, Z., Wang, G., Li, D., Yu, H., Chen, X., 2020. Accelerated dryland expansion regulates future variability in dryland gross primary production. *Nat. Commun.* 11, 1665. <https://doi.org/10.1038/s41467-020-15515-2>.
- Yao, Y., Wang, X., Li, Y., Wang, T., Shen, M., Du, M., He, H., Li, Y., Luo, W., Ma, M., Ma, Y., Tang, Y., Wang, H., Zhang, X., Zhang, Y., Zhao, L., Zhou, G., Piao, S., 2018. Spatiotemporal pattern of gross primary productivity and its covariation with climate in China over the last thirty years. *Glob. Change Biol.* 24, 184–196. <https://doi.org/10.1111/gcb.13830>.
- Yu, J., Wang, W., Chen, Z., Cao, M., Qian, H., 2025. Disentangling the dominance of atmospheric and soil water stress on vegetation productivity in global drylands. *J. Hydrol.* 657, 133043. <https://doi.org/10.1016/j.jhydrol.2025.133043>.
- Yu, X., Zhang, L., Zhou, T., Zheng, J., Guan, J., 2024. Higher atmospheric aridity-dominated drought stress contributes to aggravating dryland productivity loss under global warming. *Weather Clim. Extrem.* 44, 100692. <https://doi.org/10.1016/j.wace.2024.100692>.
- Yuan, Z., Xu, J.J., Chen, J., Wang, Y.Q., Yin, J., 2021. EVI indicated spatial-temporal variations in vegetation and their responses to climatic and anthropogenic factors in the Chinese mainland since 2000s. *J. Environ. Inform.* 40, 157–175. <https://doi.org/10.3808/jei.202100467>.
- Zhang, F., Zeng, B., Wang, P., Jiang, R., Zhang, Q., 2024a. Dominant drivers of vegetation changes in key ecological barrier of northeastern Tibetan Plateau since 2000: human impacts or natural forces? *J. Environ. Manag.* 371, 123257. <https://doi.org/10.1016/j.jenvman.2024.123257>.
- Zhang, T., Yu, G., Chen, Z., Hu, Z., Jiao, C., Yang, M., Fu, Z., Zhang, W., Han, L., Fan, M., Zhang, R., Sun, Z., Gao, Y., Li, W., 2020. Patterns and controls of vegetation productivity and precipitation-use efficiency across Eurasian grasslands. *Sci. Total Environ.* 741, 140204. <https://doi.org/10.1016/j.scitotenv.2020.140204>.
- Zhang, X., Evans, J.P., Burrell, A.L., 2024b. Less than 4% of dryland areas are projected to desertify despite increased aridity under climate change. *Commun. Earth Environ.* 5. <https://doi.org/10.1038/s43247-024-01463-v>.
- Zhang, Y., Hong, S., Liu, D., Piao, S., 2023a. Susceptibility of vegetation low-growth to climate extremes on Tibetan Plateau. *Agric. For. Meteorol.* 331, 109323. <https://doi.org/10.1016/j.agrformet.2023.109323>.
- Zhang, Y., Zhang, Y., Lian, X., Zheng, Z., Zhao, G., Zhang, T., Xu, M., Huang, K., Chen, N., Li, J., Piao, S., 2023b. Enhanced dominance of soil moisture stress on vegetation growth in Eurasian drylands. *Natl. Sci. Rev.* 10, nwad108. <https://doi.org/10.1093/nsr/nwad108>.
- Zhang, Z., Ma, X., Maeda, E.E., Lu, L., Wang, Y., Xie, Z., Li, X., Pan, Y., Huang, L., Zhao, Y., Huete, A., 2024c. Satellite observed dryland greening in Asian endorheic basins: drivers and implications to sustainable development. *Sci. Total Environ.* 922, 171216. <https://doi.org/10.1016/j.scitotenv.2024.171216>.